Electronic Supplementary Material (ESI) for Soft Matter.

Supplementary Information

Effect of Oligonucleic Acid (ONA) Backbone Features on Assembly of ONA-Star Polymer Conjugates: A Coarse-Grained Molecular Simulation Study

Joshua E. Condon[a, #], Arthi Jayaraman[a,b*]

[a]Department of Chemical and Biomolecular Engineering, Colburn Laboratory, 150 Academy Street, University of Delaware, Newark DE 19716

[b]Department of Material Science and Engineering, University of Delaware, Newark DE 19716

*Corresponding author arthij@udel.edu

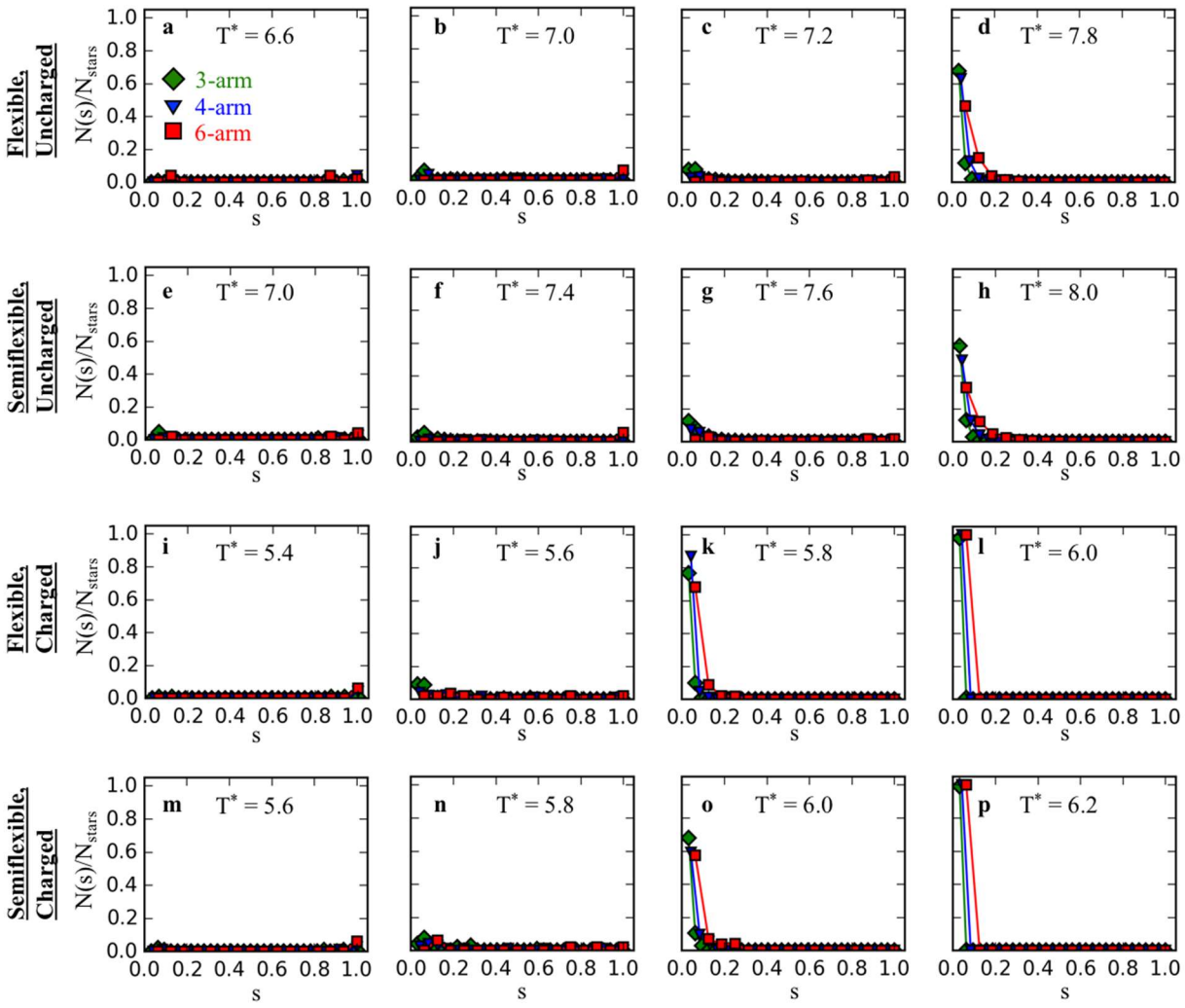

Figure S1: *(a-p) $N(s)/N_{stars}$ vs. s, where N(s) is defined as number of clusters of size s, N_{stars} is the number of ONA-star polymer conjugates in the system, and s is defined as the number of stars forming a cluster divided by the total number of stars in the system, for a range of temperatures within the assembly transition region. This plot is for C_8-G_8 systems at a volume fraction of ONA strands (ϕ_{ONA}) of 0.0032. Data for 3-arm stars are denoted by green diamonds, 4-arm stars with blue triangles, and 6-arm stars with red squares. The legend in Figure S1a holds for all plots in Figure S1. The titles on the left refer to the ONA backbone flexibility and ONA backbone charge of the systems corresponding to the plots in that row.*

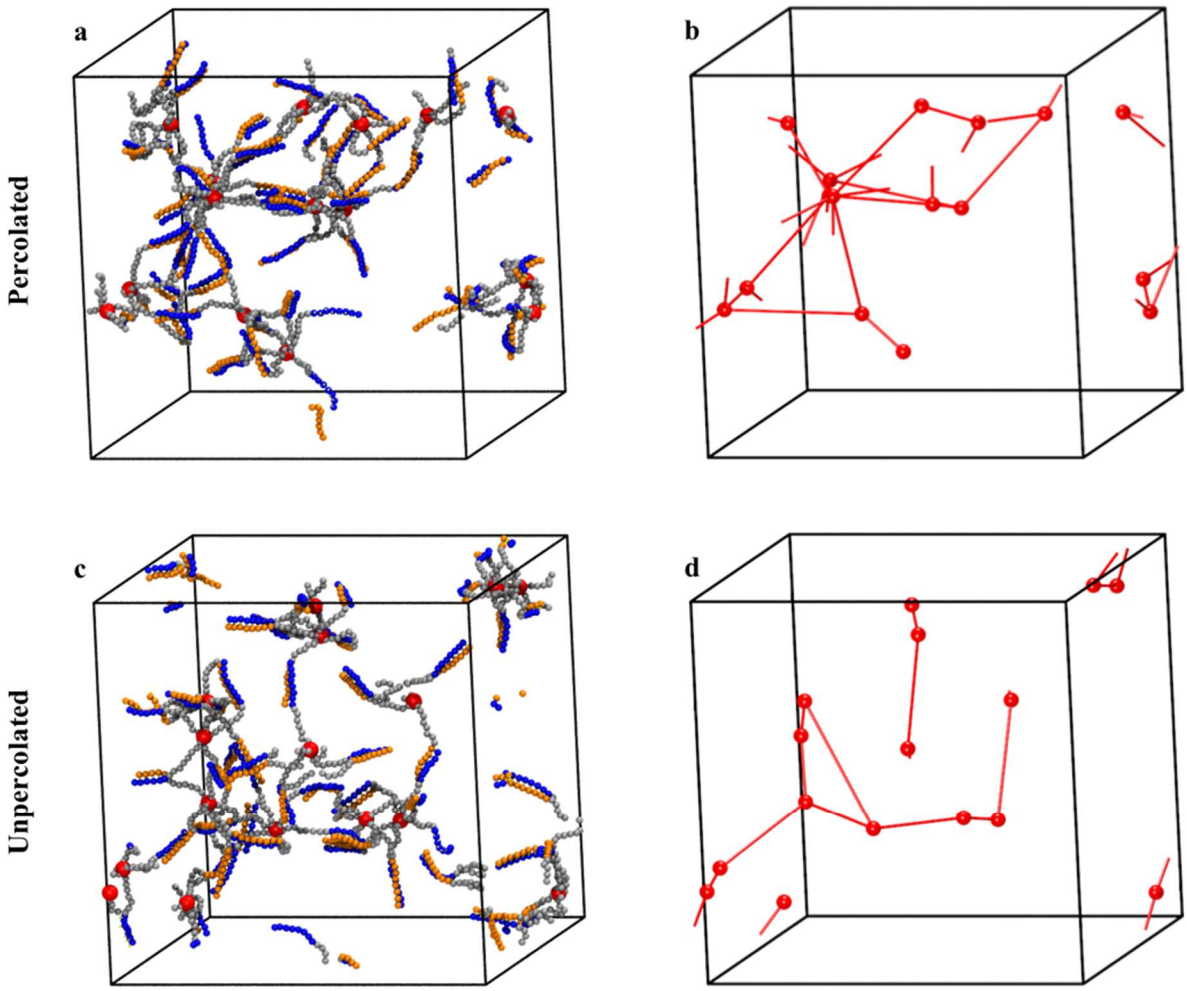

Figure S2: *(a) Simulation snapshot of* ***a percolated state*** *of 6-arm ONA-star polymer conjugate for the charged, semi-flexible ONA backbone system with C8-G8 sequence at* ϕ_{ONA} *of 0.0032 and* T^* *of 4.0 where bead colors are the same as in Figure 4 with the exception of the core (CR) beads which are enlarged and shown in red. (b) The same snapshot as Figure S2a with the polymer and backbone beads removed and the connections between ONA-star polymer conjugates shown as a red line between two CR beads. (c) The same system as Figure S2a, in* ***an unpercolated state****. (d) The same snapshot as Figure S2c with the polymer and backbone beads removed and the connections between ONA-star polymer conjugates shown as a red line between two CR beads. By evaluating the connection maps (Figures S2b and S2d), we can provide a visual means of evaluating percolation. Ion (IN) beads are not shown for clarity.*

Results for Sequence 2 ATGCTACG

In the main paper, we presented structure and thermodynamics for ONA-star polymer conjugates with C8-G8 ONA sequence. To prove that those trends in structure and thermodynamics with varying ONA backbone charge, ONA backbone flexibility, and ONA-star polymer conjugate architecture shown for C8-G8 sequence, also hold for another ONA sequence, we performed simulations with a second sequence ATGCTACG, which is both asymmetric in nucleobase sequence and has a lower G-C content of 50% compared to C8-G8.

Figure S3 and Table S1 for sequence 2 are analogous to Figure 2 and Table 1 in main paper for sequence 1. Comparing these figures and tables we see that the trends in T_m^* with varying ONA backbone charge and ONA flexibility hold for both sequences. The values of T_m^* for sequence 2 systems are lower than the corresponding sequence 1 (C_8-G_8) systems; this is expected since the G-C content is lower in sequence 2, and thus, the enthalpic driving force stabilizing the hybridized state is smaller for sequence 2.[1,2] In addition, the width of the melting transition, ΔT_m^*, is smaller for sequence 2 as compared to sequence 1, due to higher occurrences of slip (i.e. partial hybridization of some Cs in one strand with some Gs in another strand) in sequence 1 than sequence 2. Lastly, we note that in charged systems with sequence 2 ONA, at low temperatures, we observe partial hybridization between arms of the same ONA-star polymer conjugate, as shown in Figure S4 which limits the system from complete hybridization and $f_{50\%} < 1$. These occurrences are seen primarily in the charged systems because they balance out the electrostatic repulsions between the ONA strands in the arms of the ONA-star polymer conjugate.

Figure S5, Table S2, and Figure S6 for sequence 2 are analogous to Figure 3, Table 2, and Figure 4, respectively, for sequence 1 in the main paper. Again, we observe for both sequences the same trends in T_a^* with respect to ONA backbone charge, ONA flexibility, and ONA-star polymer conjugate architecture. Additionally, like ΔT_m^*, we observe a reduction in ΔT_a^* across all systems when changing the sequence from sequence 1 to sequence 2. Because assembly is inherently linked to hybridization, we expect that this reduction in ΔT_a^* is due to "slip" partial hybridization in sequence 1 systems. The simulation snapshots in Figure S6 and Figure 4 seem similar in all cases with the one noticeable difference for 6-arm charged systems. In the snapshots for sequence 2 (Figure S6f and S6h) the ONA-star polymer conjugates seem less percolated, and less regularly spaced apart as compared to the analogous systems with sequence 1 (Figure 4i and 4l). This is due to occurrences of intra-ONA-star polymer hybridization seen in charged sequence 2 systems (as shown in Figure S4) that we do not see in sequence 1 or in uncharged sequence 2 systems, which limits those sequence 2 strands from hybridizing with other ONA-star polymers in the systems and expanding the cluster. These visual observations are corroborated with results in Figures S7-S9.

Figure S7 shows the normalized cluster size distribution for a range of temperatures around T_a^* for sequence 2 systems. Comparing Figure S7 (sequence 2) to Figure 5 (sequence 1), we see that the trends in

cluster size around T_a^* hold for both sequences studied. Again, the only exception is that in the case of the charged sequence 2 systems because of partial hybridization within the same ONA-star polymer conjugate we see several smaller clusters at low temperatures that are likely kinetically trapped. Comparing Figure S8 (sequence 2) to Figure 6 (sequence 1), we see that percolation does not occur at low temperatures for charged sequence 2 systems; the dominance of several small clusters that are likely kinetically trapped prevents percolation from happening. Percolation seems to occur with higher probability near the melting transition temperatures because of the increased likelihood of those intra-molecular partially hybridized bases melting and hybridizing with other star polymer molecules. Lastly, comparing Figure S9 (sequence 2) to Figure 7 (sequence 1), we see that at temperatures below T_a^*, the first peak in the core-core pair correlation curve is shifted to higher interparticle distance for sequence 2 than sequence 1. This could be because there is inter-ONA star polymer partial hybridization in sequence 1 and the hybridized duplexes need not be directionally matched (i.e. 5' and 3' end are not distinguished in this CG model); these allow the CR core beads to approach one another at closer distances than if the hybridized state was directional as in sequence 2 systems. There does not appear to be any major difference in the dispersion of ONA-star polymer conjugates between sequence 1 and sequence 2 for temperatures above T_a^*. In addition, trends in $g(r)_{core\text{-}core}$ with respect to ONA charge, ONA flexibility, and ONA-star polymer conjugate architecture are similar for sequence 1 and sequence 2, except for the charged sequence 2 systems at low temperatures. As stated above, at these low temperatures, the charged sequence 2 systems are likely kinetically trapped in a state of several small clusters rather than one or two large clusters which prevents longer range order from occurring.

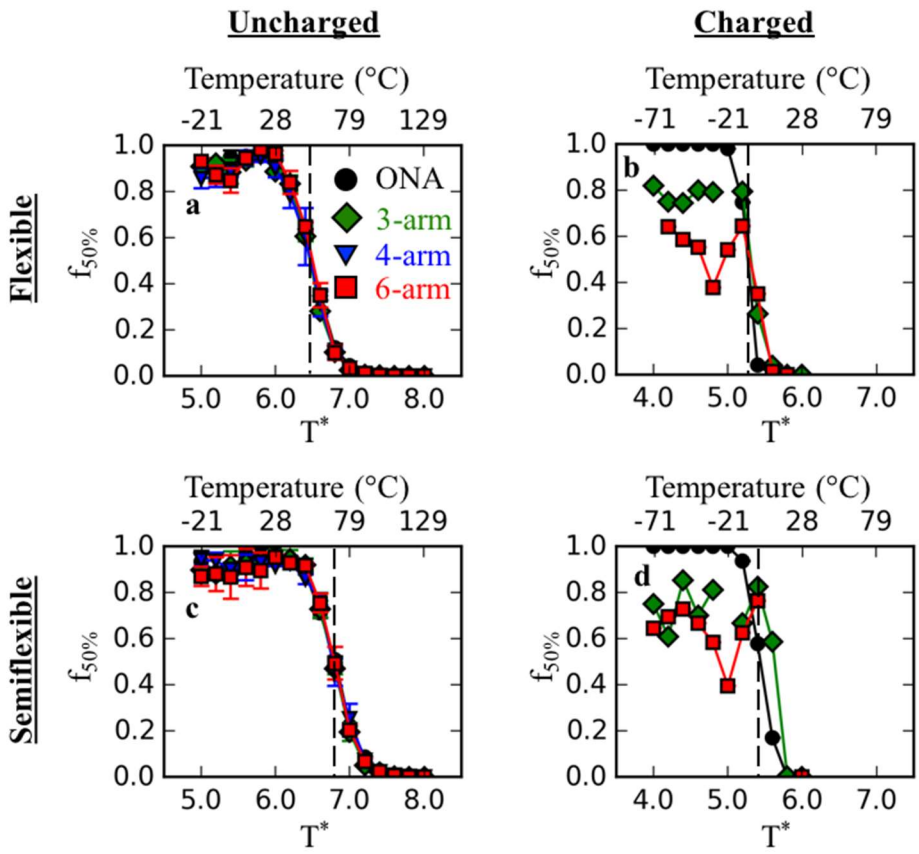

Figure S3: *(a-d) Fraction of oligonucleic acid (ONA) strands that have at least fifty percent of possible H-bonds formed ($f_{50\%}$) as a function of reduced temperature (T^*) for free ONA (black circles), 3-arm stars (green diamonds), 4-arm stars (blue triangles), and 6-arm stars (red squares) for* ***sequence 2*** *at a volume fraction of ONA strands (ϕ_{ONA}) of 0.0032. The legend in Figure S3a holds for all plots in Figure S3. The titles along the top of the figure refer to the ONA backbone charge of the systems corresponding to the plots. The titles along the left side of the figure refer to the ONA backbone flexibility of the systems corresponding to the plots. In all plots, we show the reduced temperature in the x-axis and the corresponding temperature in degree Celsius on the top of the plot. The black dashed lines in all plots denote the reduced melting temperature, T_m^*, for the free ONA case.*

Table S1: *Melting temperature, T_m^* and width of the melting transition, ΔT_m^*, for free ONA and ONA-star polymer conjugate systems for* ***sequence 2*** *with varying star polymer architecture, ONA backbone charge and ONA backbone flexibility.*

ONA Backbone Charge	ONA Backbone Flexibility	Architecture	T_m^*	ΔT_m^*
Uncharged	**Flexible**	Free ONA	6.49	0.77
		3-arm	6.47	0.84

		4-arm	6.47	0.80
		6-arm	6.50	0.70
	Semiflexible	Free ONA	6.81	0.82
		3-arm	6.78	0.78
		4-arm	6.77	0.89
		6-arm	6.78	0.73
Charged	**Flexible**	Free ONA	5.27*	0.23
		3-arm	5.31*	**
		6-arm	**	**
	Semiflexible	Free ONA	5.44*	0.46
		3-arm	5.63*	**
		6-arm	**	**

** Melting temperature and width of melting transition values listed for these charged systems here are based on a set of single replicate simulations for each temperature instead of the typical average over a set of 3 replicate simulations for each temperature that are used for the rest of the systems in the paper and supplementary information.*

*** We do not report a value for the melting temperature and width of melting transition here because of the high propensity of kinetic trapping at low temperatures in the charged 6-arm sequence 2 systems presented here. The melting curves are presented in Figure S3.*

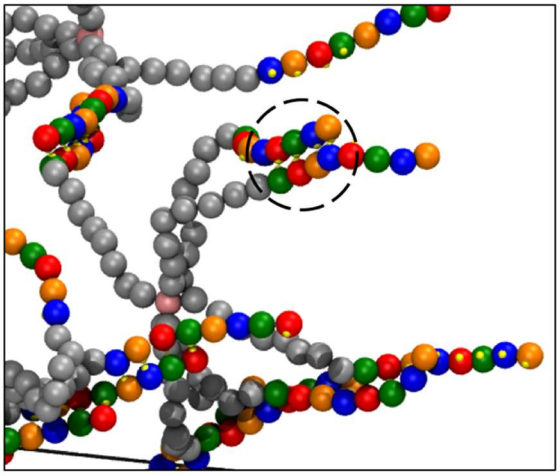

Figure S4: *Visualization of partial hybridization of ONA strands within the same ONA-star polymer conjugate for the sequence 2, 6-arm charged semiflexible ONA-star polymer conjugate system at* $T^* = 4.0$*. This behavior occurs for the sequence 2 charged systems and reduces* $f_{50\%}$ *at low temperatures, increases the number of small clusters that form at low temperatures, and prevents percolation from occurring at low temperatures as well.*

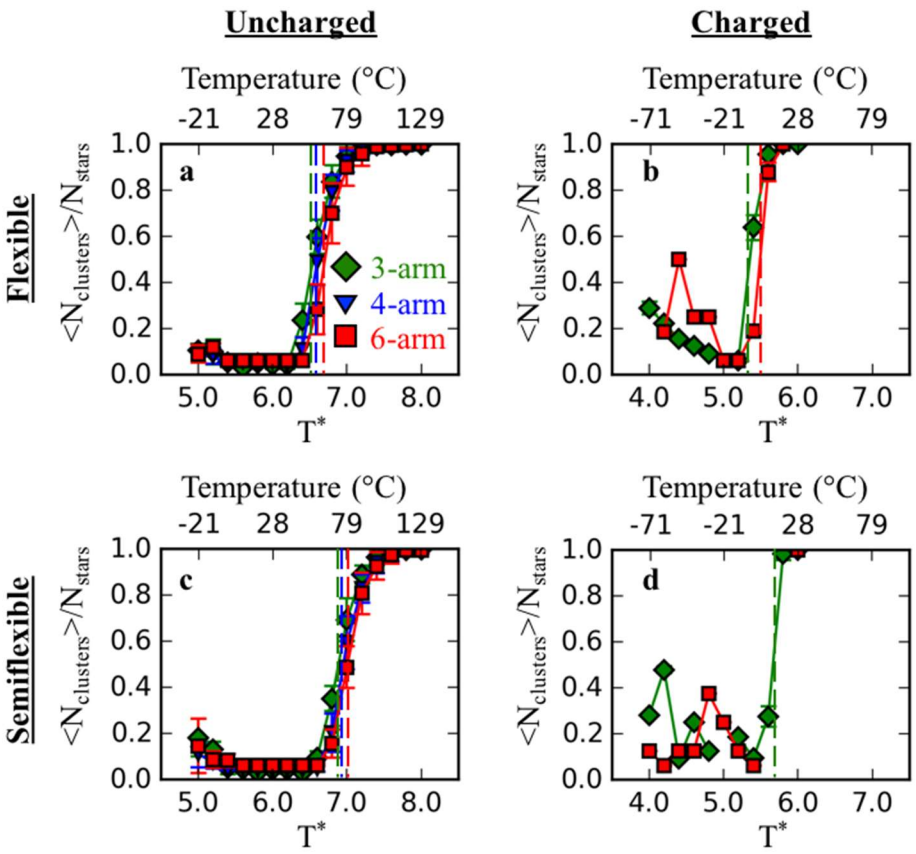

Figure S5: *(a-d) Average number of clusters (<$N_{clusters}$>) normalized by the total number of stars in each system (N_{stars}) as a function of temperature for 3-arm stars (green diamonds), 4-arm stars (blue triangles), and 6-arm stars (red squares)* ***for sequence 2*** *at a volume fraction of ONA strands (ϕ_{ONA}) of 0.0032. The legend in Figure S5a holds for all plots in Figure S5. The titles along the top of the figure refer to the ONA backbone charge of the systems corresponding to the plots. The titles along the left side of the figure refer to the ONA backbone flexibility of the systems corresponding to the plots. The dashed lines in all plots denote the reduced assembly transition temperature, T_a^*, for the corresponding architecture.*

Table S2: *Assembly transition temperature, T_a^*, and assembly transition width, ΔT_a^*, for ONA-star polymer conjugates* ***for sequence 2*** *with respect to ONA backbone charge, ONA backbone flexibility, and ONA-star polymer conjugate architecture.*

ONA Backbone Charge	ONA Backbone Flexibility	Architecture	T_a^*	ΔT_a^*
Uncharged	**Flexible**	3-arm	6.55	0.65
		4-arm	6.61	0.59
		6-arm	6.70	0.56

	Semiflexible	3-arm	6.89	0.62
		4-arm	6.95	0.66
		6-arm	7.01	0.68
Charged	**Flexible**	3-arm	5.35*	**
		6-arm	**	**
	Semiflexible	3-arm	5.66*	**
		6-arm	**	**

**Note: Assembly transition temperature and width of assembly transition values listed for the charged sequence 2 systems are approximate and based on a set of single replicate simulations for each temperature instead of the typical set of 3 replicate simulations for each temperature that are used for the rest of the systems in the paper and supplementary information. We chose to do only one simulation trial because of the high propensity for the system to be kinetically trapped at low temperature.*

*** We do not report a value for the assembly transition temperature and width of assembly transition here because of the high propensity of kinetic trapping at low temperatures in the charged 6-arm sequence 2 systems presented here. The assembly transition curves are presented in Figure S5.*

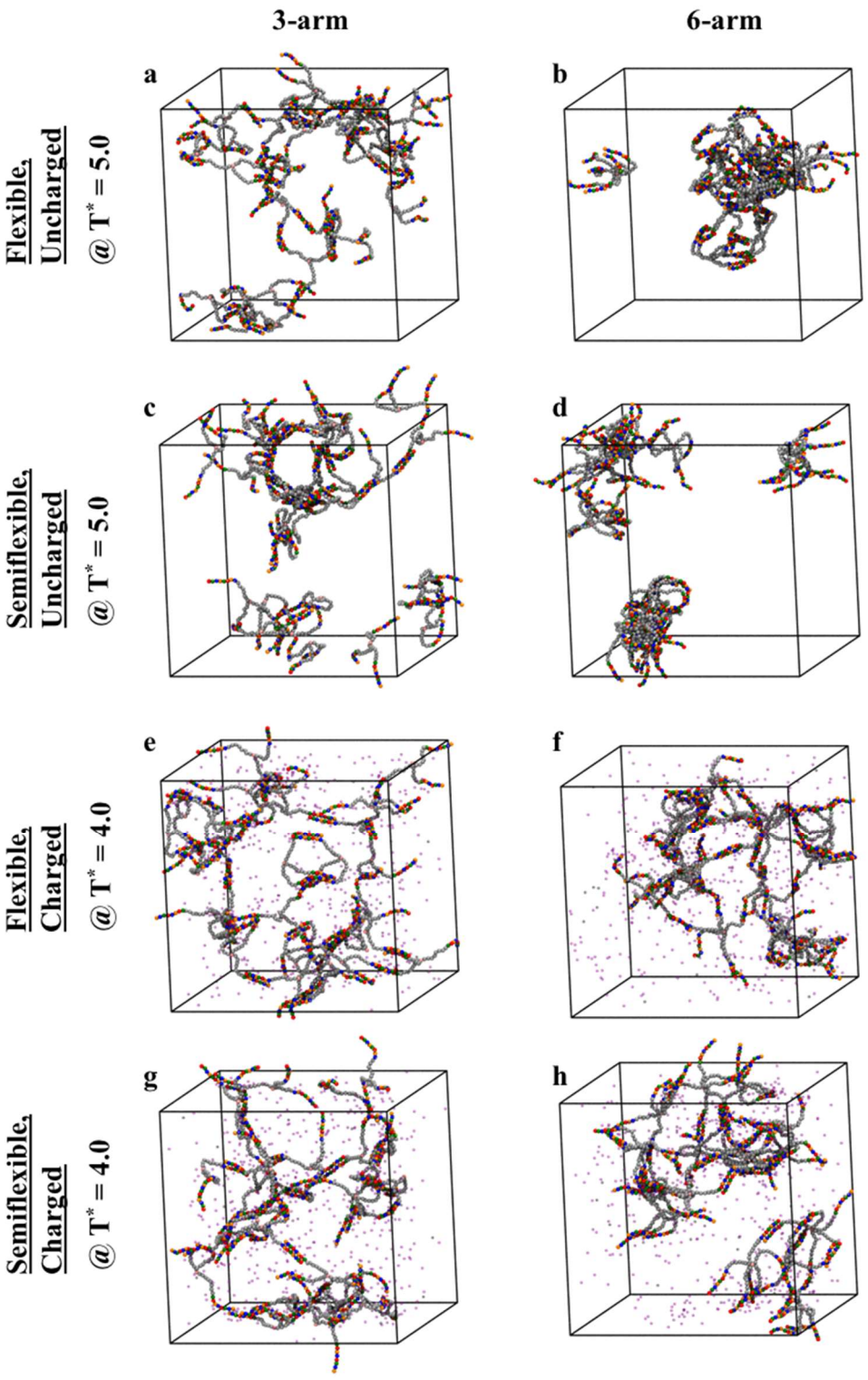

Figure S6: *(a-h) Simulation snapshots of assembled ONA-star polymer conjugates* ***for sequence 2*** *at a volume fraction of ONA strands (ϕ_{ONA}) of 0.0032. The titles along the top of the figure refer to the ONA-star polymer conjugate architecture. The titles along the left side of the figure refer to the ONA backbone*

flexibility and ONA backbone charge of the systems corresponding to the plots. The temperatures at which the snapshots were taken are listed underneath the titles along the left side of the figure. In each system, the backbone beads (BB) are represented by the colors red, green, orange, and blue for type A, T, C, and G, respectively. The polymer (PL) beads are represented by the color grey, and the ion (IN) beads in the charged ONA backbone systems are represented by the colors purple and black for +1 and -1 valencies, respectively. In the charged systems, these ion beads include both the neutralizing +1 charge ions as well as +1 and -1 ions to represent 1mM of monovalent salt.

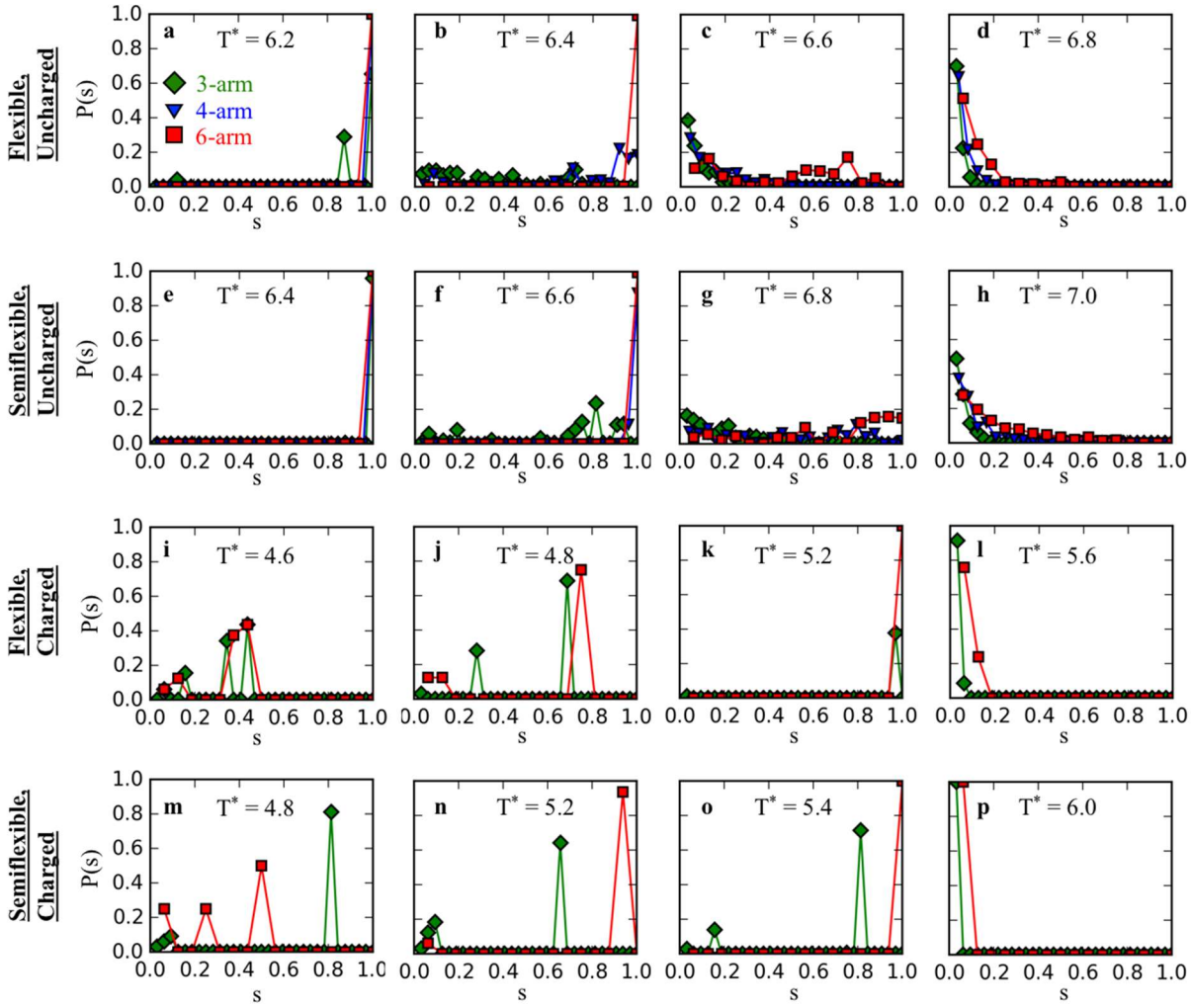

Figure S7: *(a-p) Normalized probability distribution of clusters of size* ***s*** *denoted as P(s), for a range of temperatures within the assembly transition region* ***for sequence 2*** *at a volume fraction of ONA strands (ϕ_{ONA}) of 0.0032. Data for 3-arm stars are denoted by green diamonds, 4-arm stars with blue triangles, and 6-arm stars with red squares. The legend in Figure S7a holds for all plots in Figure S7. The titles on the*

left refer to the ONA backbone flexibility and ONA backbone charge of the systems corresponding to the plots in that row.

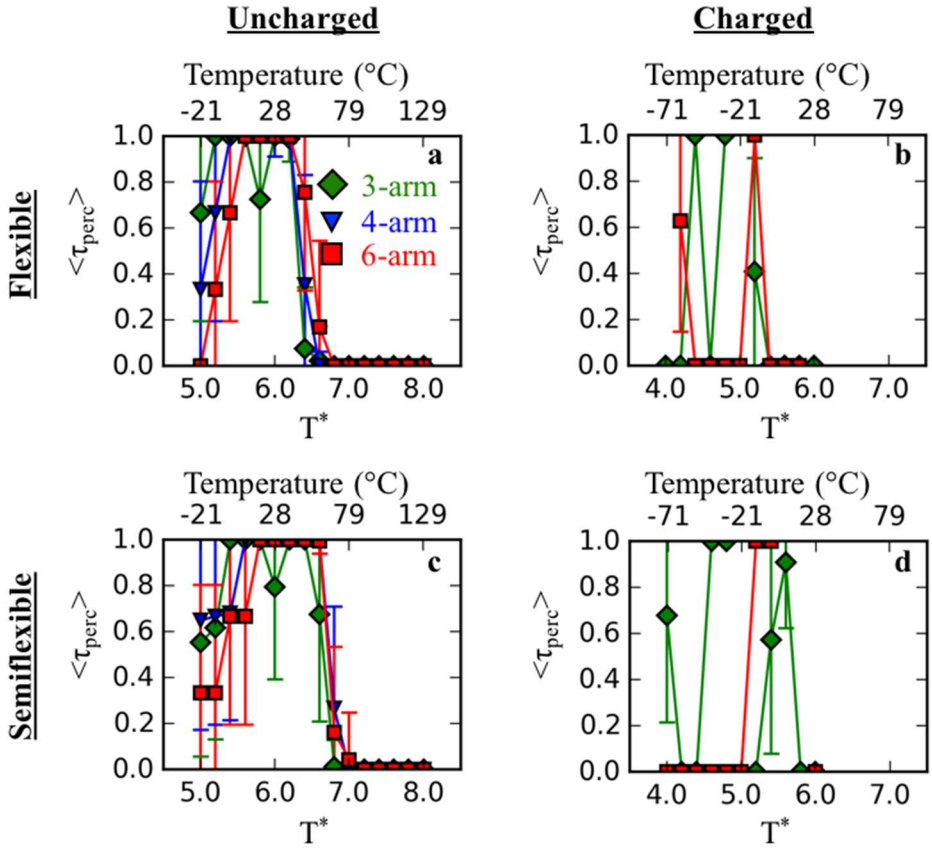

Figure S8: *(a-d) Fraction of simulation frames spent in a percolated state (<τ_{perc}>) as a function of temperature for 3-arm stars (green diamonds), 4-arm stars (blue triangles), and 6-arm stars (red squares)* ***for sequence 2*** *at a volume fraction of ONA strands (ϕ_{ONA}) of 0.0032. The legend in Figure S8a holds for all plots in Figure S8. The titles along the top of the figure refer to the ONA backbone charge of the systems corresponding to the plots. The titles along the left side of the figure refer to the ONA backbone flexibility of the systems corresponding to the plots.*

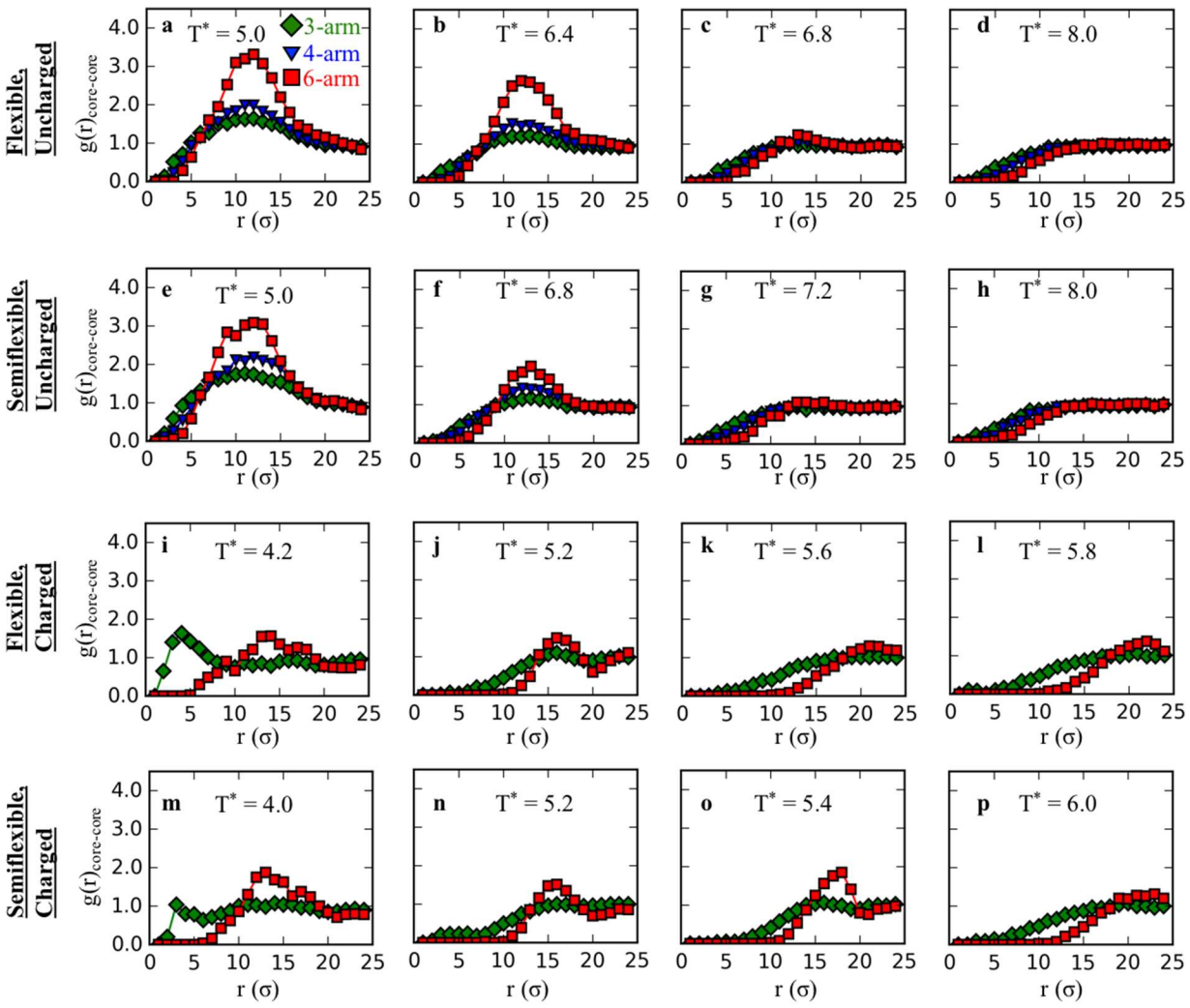

Figure S9: *(a-p) Radial distribution function among core (CR) beads ($g(r)_{core\text{-}core}$) as a function of separation distance r (having units of σ)* ***for sequence 2*** *at a volume fraction of ONA strands (ϕ_{ONA}) of 0.0032. Data for 3-arm stars are denoted by green diamonds, 4-arm stars with blue triangles, and 6-arm stars with red squares. The legend in Figure S9a holds for all plots in Figure S9. The titles on the left refer to the ONA backbone flexibility and ONA backbone charge of the systems corresponding to the plots in that row.*

References:

1. P. Yakovchuk, E. Protozanova and M. D. Frank-Kamenetskii, *Nucleic Acids Research*, 2006, **34**, 564-574.
2. A. Seifpour, S. R. Dahl, B. Lin and A. Jayaraman, *Molecular Simulation*, 2013, **39**, 741-753.